INTERNATIONAL JOURNAL OF PRECISION ENGINEERING AND MANUFACTURING Vol. 16, No. 9, pp. 1999-2004 AUGUST 2015 / 1999
DOI: 10.1007/s12541-015-0260-5 ISSN 2234-7593 (Print) / ISSN 2005-4602 (Online)

Investigation of Localized Heating Characteristics in Selective Ultrasonic Imprinting

Woosin Jung[1,2], Hyun-Joong Lee[1], and Keun Park[1,#]

1 Department of Mechanical System Design Engineering, Seoul National University of Science and Technology, 232, Gongneung-ro, Nowon-gu, Seoul, 139-743, South Korea
2 FAB Equipment Division, SEMES Co. Ltd., 77, 4sandan 5-gil, Jiksan-eup, Seobuk-gu, Cheonan-si, Chungcheongnam-do, 331-814, South Korea
Corresponding Author / E-mail: kpark@seoultech.ac.kr, TEL: +82-2-970-6358, FAX: +82-2-974-8270

KEYWORDS: Ultrasonic imprinting, Selective ultrasonic imprinting, Localized heating, Micropattern replication, Finite element analysis

Ultrasonic imprinting is a patterning technology in which ultrasonic vibration energy is used to soften the surface of thermoplastic polymer to allow the formation of micropatterns. Compared with other patterning technologies, ultrasonic imprinting has the advantages of short cycle time and low energy consumption. This study deals with the selective ultrasonic imprinting process, which provides higher flexibility in developing versatile micropatterns. Selective ultrasonic imprinting uses a profiled mask film by which ultrasonic waves are transferred from an ultrasonic horn to a target polymer film. The target polymer film is locally softened in the regions in contact with the mask film, so that micropatterns can be selectively replicated in these regions. In this study, this localized heating mechanism is numerically investigated through structural-thermal-coupled finite element analysis, by effectively connecting transient structural and heat transfer analyses. This coupled simulation was performed to investigate the localized heating mechanism of the selective imprinting using an E-shaped mask, and then compared with experimental findings. Micropattern replication was then performed using an arbitrarily shaped logo, with which differentiation of optical transparency could be obtained.

Manuscript received: February 22, 2015 / Revised: March 28, 2015 / Accepted: June 4, 2015

1. Introduction

In recent years, ultrasonic waves have been used to facilitate plasticization of thermoplastic polymer by converting ultrasonic vibration energy into thermal energy.[1] Thus, the ultrasonic vibration energy can act as an auxiliary heat source in various polymer processing technologies. Owing to the rapid and localized heating capability of ultrasonic energy, it has been utilized in micromolding of thermoplastic polymers using processes such as hot embossing[2-4] and injection molding.[5,6]

The use of ultrasonic energy as an auxiliary heat source has changed into the development of ultrasonic imprinting, which uses ultrasonic energy as its main energy source by inducing microscale ultrasonic vibration on the polymer surface.[7,8] In this way, ultrasonic vibration energy is used to soften polymer surfaces locally so that micropatterns can be replicated on thermoplastic polymer. Owing to its low energy consumption and short cycle time, ultrasonic imprinting provides higher efficiency in developing micropatterns on thin polymer films, as compared with the conventional hot embossing or injection molding processes.

Recently, the ultrasonic imprinting process was further developed to include replication of micropatterns on areas of arbitrary shapes; a process called selective ultrasonic imprinting.[9] In this advanced imprinting process, a mask film of a particular shape is used to transfer ultrasonic waves from an ultrasonic horn to a target film. Thus, micropatterns could be selectively replicated in the specified regions in contact with the mask film. In previous work of the authors, effects of imprinting conditions were investigated experimentally in terms of micropattern replication quality, not only of the masked area, but also of the unmasked area.[9,10]

In this study, the localized heating mechanism of selective ultrasonic imprinting was numerically investigated through structural-thermal-coupled finite element (FE) analysis. Considering that the ultrasonic imprinting process can be divided into two steps (vibration and heating),[11] structural and thermal FE analyses were modeled and performed for each stage. This coupled simulation was performed for the selective imprinting process using an E-shaped mask, and was compared with the relevant experimental findings in terms of the effect of imprinting conditions on the localized heating capability. The selective imprinting process was then adapted to use a mask with an arbitrarily shaped logo, from which micropatterns were successfully replicated on the target region of the polymer. The replicated micropatterns thereby allowed the differentiation of optical transparency.

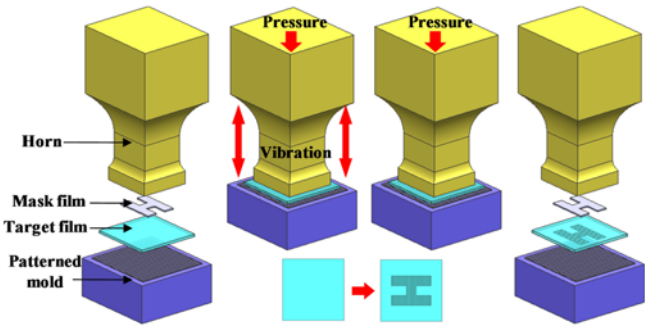

Fig. 1 Schematic description of the selective imprinting process[9]

2. Overview of Selective Ultrasonic Imprinting

For ultrasonic imprinting, ultrasonic vibration energy is used to generate localized deformation of a polymer surface, and to induce frictional heat between an ultrasonic horn and a thermoplastic polymer film. A micropatterned mold is placed below the polymer film. The ultrasonic vibration is transferred from the horn to the mold through the polymer film. The surface region of the target film is then softened by the repetitive deformation energy and frictional heat so that the mold micropatterns can be replicated on the polymer surface.

On the other hand, in the selective imprinting, a mask film with an arbitrary profile is used. Fig. 1 shows a configuration of the selective imprinting process in which ultrasonic waves can be selectively transferred through the mask film by placing the mask film between the horn and target polymer film.[9] The target film is then locally softened in the regions in contact with the mask film, so that micropatterns are selectively replicated in these regions. Therefore, this approach provides versatility to create a variety of micropatterns using a single micropatterned mold, by fabricating and inserting the corresponding mask films.

3. Numerical Simulation for the Selective UIL Process

3.1 Simulation overview

The ultrasonic imprinting process can be divided into two steps: vibration and heating. To simulate the vibration step, a structural FE analysis was conducted to calculate the deformation fields inside the polymer film, caused by the propagated ultrasonic wave. To simulate the heating step, a thermal FE analysis was conducted to predict the temperature rise inside the polymer film, by imposing the ultrasonic deformation energy as a heat source.

Fig. 2 shows an analysis domain and the related simplified models for the selective imprinting process. A negative E-shaped mask film was designed with a size of 22×22×0.4 mm^3, as illustrated in Fig. 2(a). This analysis domain was simplified by using a two-dimensional sectional model containing the mask and target films. Fig. 2(b) and 2(c) show the intermediate simplified model and the final simplified domain, respectively. The mask material was AA-1050, and the target film was polyethylene terephthalate (PET). The material properties and thicknesses of both films are summarized in Table 1. A micropatterned mold was located below the target film on which a number of micro-prism patterns were engraved (400 mm pitch and 170 mm height). An

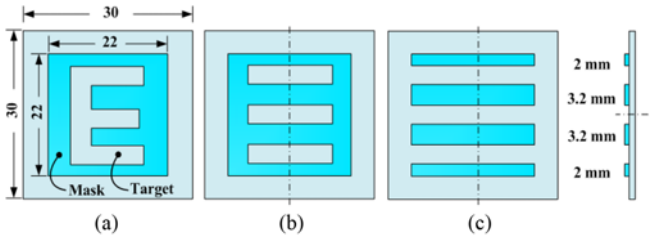

Fig. 2 FE analysis domain for the selective UIL with an E-shaped mask: (a) the original domain, (b) the intermediate simplified model, and (c) the final simplified domain with a side view

Table 1 Material properties of AA-1050 and PET films

Material properties	AA-1050	PET
Elastic modulus (GPa)	69	1.68
Poisson's ratio	0.33	0.4
Density (kg/m^3)	2705	1330
Thermal conductivity (W/m-K)	227	0.15
Specific heat (J/kg-K)	900	1200
Thickness (mm)	0.4	0.3

ultrasonic horn was located above the mask film, and its vibration effect was imposed as a form of external force. ANSYS™ was used in the structural-thermal coupled FE analysis, and the detailed simulation results are described in the following sections.

3.2 Simulation for the vibration step

In the vibration step, ultrasonic excitation induces a polymer film to repetitive deformation. This deformation fields (u) can be obtained by solving Eq. (1), a discretized FE motion equation:

$$\mathbf{M}\ddot{u}(t)+\mathbf{C}\dot{u}(t)+\mathbf{K}u(t)=F(t) \tag{1}$$

where **M**, **C**, and **K** are mass, damping and stiffness matrices, respectively. Transient structural analysis is then conducted by applying the ultrasonic excitation force as a half-sinusoidal form, expressed in Eq. (2):[11]

$$F(t)=\begin{cases} F_0\sin(2\pi ft), & \left(n-\frac{1}{2}\right)T\le t\le nT \\ 0, & (n-1)T\le t\le\left(n-\frac{1}{2}\right)T \end{cases} \tag{2}$$

where F_0 is the amplitude of the excitation force, f is the excitation frequency, T is the time period, and n is the number of cycles.

The amplitude (F_0) and frequency (f) for the ultrasonic excitation were determined (25.9 N and 20 kHz, respectively) from experimental observations. This compressive force was applied on the top surfaces of the mask film in the structural FE analysis, as shown in Fig. 3(a). DOF constraints were given for the regions in contact with the micropatterned mold, and these DOF constraints are indicated by red dots in Fig. 3(a).

Fig. 3(b) illustrates the change of the equivalent strain distributions during a loading cycle (T/16~T/2), showing that the strain concentrations occurred in the bottom regions in contact with the micropatterned mold, only in the masked area. This indicates that ultrasonic waves were

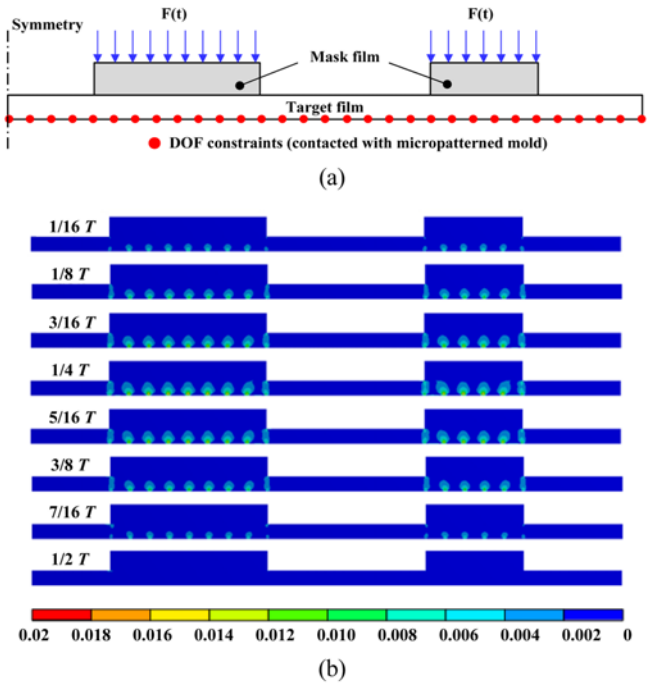

Fig. 3 Structural FE analysis for the vibration step: (a) boundary conditions, and (b) change of the effective strain distributions

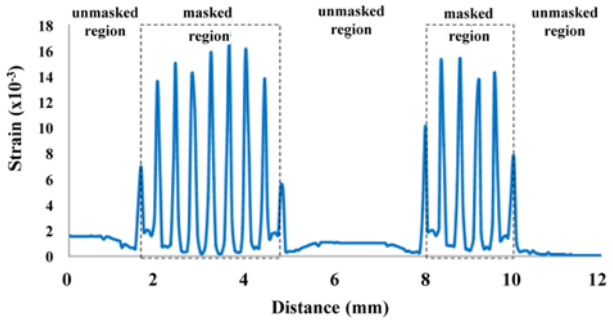

Fig. 4 Profile of the effective strain on the bottom surface at $T/4$

being transferred to the target polymer film through the mask film; therefore, only masked regions were affected by the ultrasonic excitation.

Fig. 4 shows the effective strain profile on the bottom surface at $T/4$. It can be seen that strain peaks were observed at contact points in the masked regions while no remarkable change was observed in the unmasked regions. These strain peaks in the masked regions were higher than 0.013, which is 10 times larger than that in the unmasked regions. This localized strain concentration is expected to induce localized heating, which will be discussed in the next section.

3.3 Simulation for the heating step

In the heating step, the local strain concentration in the masked regions induces heat generation due to repetitive deformation. This heat generation rate (Q) can be calculated from Eq. (3):[12]

$$Q = \pi f \varepsilon_0^2 E \sin\delta \tag{3}$$

where ε_0, E and δ are the strain amplitude, elastic modulus, and loss

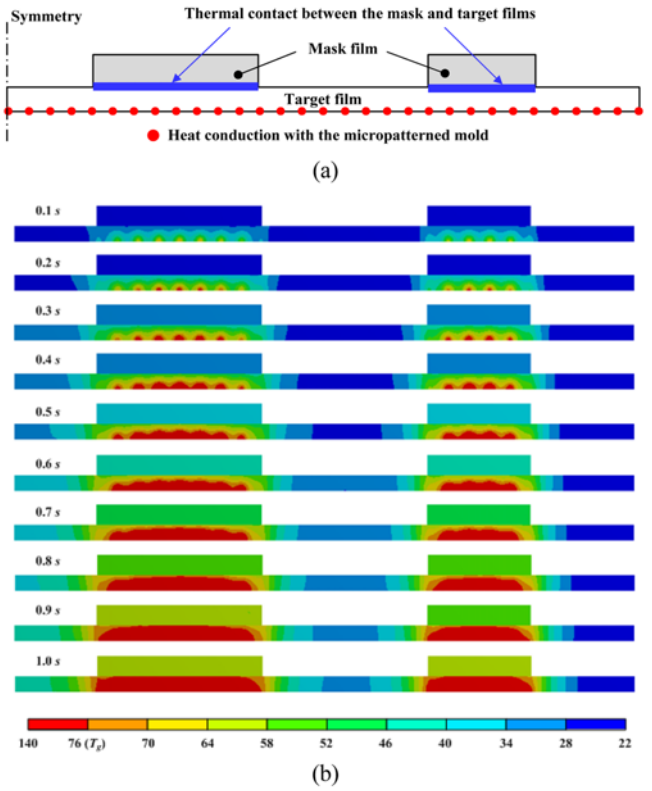

Fig. 5 Thermal FE analysis for the heating step: (a) boundary conditions, and (b) change of the temperature distribution (unit: °C)

angle of the polymer material, respectively.

Therefore, the locally deformed regions act as separate heat sources in the heating step. Transient heat-transfer analysis was then conducted by applying this heat generation, as expressed in Eq. (4):

$$\nabla^2[k(T)T] + Q = \rho C(T)\frac{\partial T}{\partial t} \tag{4}$$

where $k(T)$ and $C(T)$ are the thermal conductivity and specific heat of each material, which were regarded as functions of temperature in the case of PET film.[13]

Fig 5(a) shows thermal boundary conditions for the heat transfer analysis. The heat generation rate was calculated using Eq. (3) from the structural analysis results. The loss angle (δ) of the PET film was set to 0.559, which was measured from a rotational rheometer analysis. The thermal contact conductance between the mask and target films was set to 400 W/m^2·K. To consider heat conduction from the PET film to the micropatterned mold, the mold was also included in the heat transfer analysis although it was not displayed in Fig. 5(a). The mold material was stainless steel (SS-303), and its thermal conductivity, density, and specific heat were 16.2 W/m·K, 8000 kg/m^3, and 500 J/kg·K, respectively. The heat convection coefficient was set to 5.0 W/m^2-K for all free surfaces, including the top surfaces of the mask film and the free surfaces of the target film, that is, all outer surfaces except for the contacted regions with the mask film or micropatterned mold.

Fig. 5(b) shows the change of temperature distributions during 1.0 s vibration time with an increment of 0.1 s. Considering that the glass transition temperature (T_g) of the PET film was 76°C, the temperature

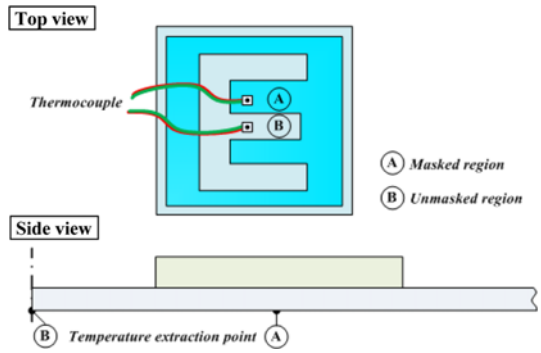

Fig. 6 Temperature measurement locations during imprinting

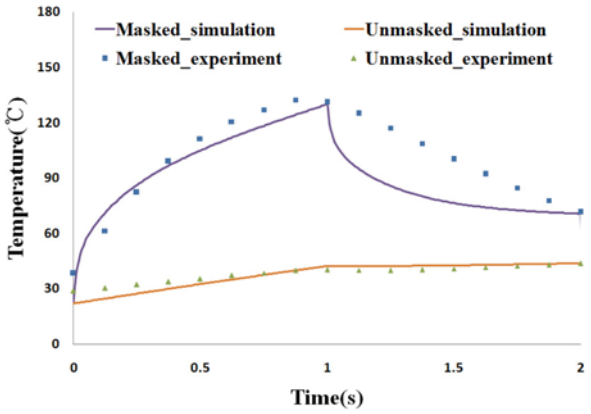

Fig. 7 Comparison of temperature variations of the masked and unmasked regions

contour was adjusted to indicate the regions with temperature higher than T_g as red. It is noted that the local heating began at the contact points on the bottom surface, and then transferred upward into the masked regions. At 1.0 s vibration time, temperatures in all the masked regions reached the target temperature (T_g) uniformly, while the unmasked regions did not show a remarkable temperature increase. This indicates that the masked region could be locally heated by the localized deformation owing to the process of selective ultrasonic imprinting.

3.4 Experimental verification

To verify the reliability of the proposed simulation, ultrasonic imprinting experiments were performed using the E-shaped mask film. All imprinting conditions were set to be the same as the simulation conditions: 0.4 MPa imprinting pressure and 1.0 s vibration time. Thermocouples were installed for temperature measurement in the masked region (marked 'A' in Fig. 6) and the unmasked regions (marked 'B' in Fig. 6). The measured temperature profiles are plotted in Fig. 7, and are compared with those from simulation. It can be seen that both simulation and experimental results were similar in overall trends that the masked region (A) showed a remarkable temperature increase unlike the unmasked region (B). The peak temperatures at both locations after 1.0 s vibration are compared in Table 2. Considering that the temperature deviations between the results in simulation and experiment were around 7°C, it could be concluded that the proposed coupled simulation

Table 2 Comparison of temperatures at locations A and B (unit: °C)

Location	Simulation	Experiment	Error
A	131.0	137.9	6.9
B	42.4	35.1	-7.3

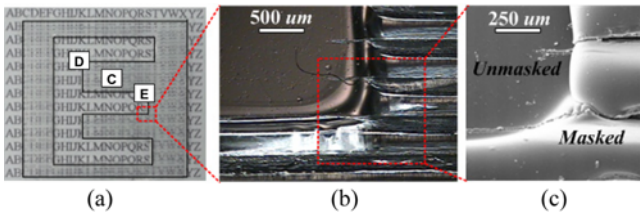

Fig. 8 Photographs of the replicated micropatterns: (a) replicated film, (b) optical microscope image, and (c) SEM image

provided a reliable estimation of localized temperature rise in the selective ultrasonic imprinting process.

4. Selective Ultrasonic Imprinting Using Negative Masks

4.1 Micropattern replication on an E-shaped region

Based on the simulation results in Section 3, selective imprinting was performed to replicate micropatterns using the E-shaped mask. The mask was fabricated with the dimensions given in Fig. 2, and the resulting mask area was 300 mm^2. Imprinting experiments were conducted at room temperature, and imprinting conditions were set to be the same as given in the previous section. A prism-patterned mold was fabricated and used in the imprinting experiments, of which height and pitch were 170 mm and 400 mm, respectively.

Fig. 8(a) shows a photograph of the patterned film placed on a background sheet with printed letters. It can be seen that the masked region showed lower transparency than the unmasked region, and that the background letters were not clearly seen in the masked region. This result indicates that micropatterns were selectively replicated in the masked region so that transparency was degenerated due to the developed micropatterns in this region. Figs. 8(b) and 8(c) illustrate an optical microscope image and scanning electron microscope (SEM) image for the boundary region, showing that micropatterns were well developed only in the masked region.

To investigate the effect of imprinting conditions on the replication quality, selective imprinting experiments were performed with a variation in vibration time: 0.5, 0.75, 1.0, and 1.5 s. Figs. 9(a) through 9(c) show photographs of the developed micropatterns in various regions (regions C, D, and E in Fig. 8(a)), with an increment of vibration time. Fig. 9(a) compares developed micropatterns in the masked region (region C), which shows that the micropatterns were not fully developed when the vibration time was less than 1.0 s. This result shows good accordance with the results in Fig. 5, that the temperature in the masked region increased to reach higher than T_g after 1.0 s vibration time. Similar trends, that 1.0 s vibration time ensured enough micropattern replications, were observed in the boundary regions (regions D and E). However, an excessive vibration time (1.5 s) resulted in micropattern replication even in the unmasked regions, as marked in Figs. 9(b) and

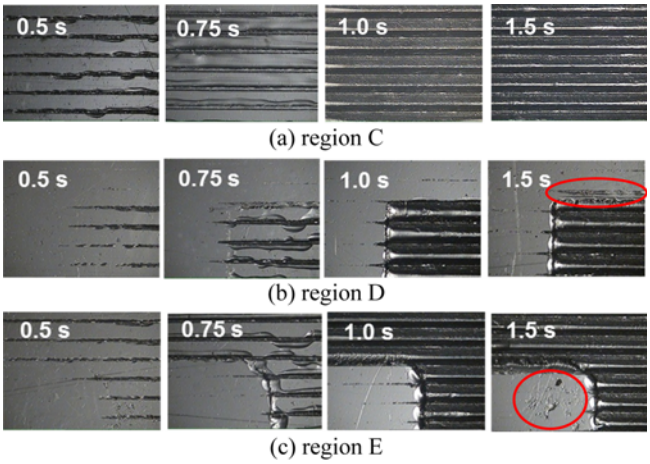

Fig. 9 Comparison of micropattern replications in various regions with an increase in vibration time

9(c). This undesired pattern replication was caused by the temperature rise in the unmasked regions when the ultrasonic energy was applied much longer than necessary.

4.2 Micropattern replication on an arbitrary-shaped logo

The proposed selective imprinting process was further applied to micropattern replication on an arbitrary shape. Fig. 10(a) shows a mask film with the SeoulTech logo. The mask was fabricated from an AA-1050 sheet with a thickness of 0.4 mm. The outer diameter of the mask was 32 mm, and the corresponding mask area was 605.3 mm^2. Because this area is twice as large as that of the previous mask, the vibration time was set in a higher range, from 3.0 s to 5.0 s. The imprinting pressure and mold temperature and were set to 0.6 MPa and 70ºC, respectively. Ultrasonic imprinting experiments were then performed using PET films with the size of 40×40×0.3 mm^3.

Fig. 10(b) shows the PET film subjected to 4.0 s vibration time. The film transparency degenerated in the masked region, due to light scattering from the developed micropatterns. To compare the transparency quantitatively, imprinting experiments were performed with a vibration in vibration time: 3.0, 4.0 and 5.0 s. Fig. 10(c) compares the measured optical transmittance profiles across the section F-F'. It was observed that the masked region showed relatively high transmittance (more than 25%) at 3.0 s vibration time, which indicates that the micropatterns were not developed enough to reduce optical transmittance. In contrast, for the cases of 4.0 and 5.0 s vibration times, low transmittance values (less than 10%) were measured in the masked region. However, when the vibration time was 5.0 s, the transmittance values were also reduced near mask boundaries even in the unmasked regions. This transmittance reduction is due to flash generation near the mask boundary when excessive imprinting conditions were applied.

Fig. 11 shows measured surface profiles of micropatterns at various locations at 4.0 s vibration time. It is observed that micropatterns were successfully replicated only in the masked region without excessive imprinting in the unmasked regions. Considering that the replication quality shows apparent differences across the mask boundaries, it can be concluded that the selective ultrasonic imprinting could replicate micropattern on arbitrary shapes when appropriate imprinting conditions

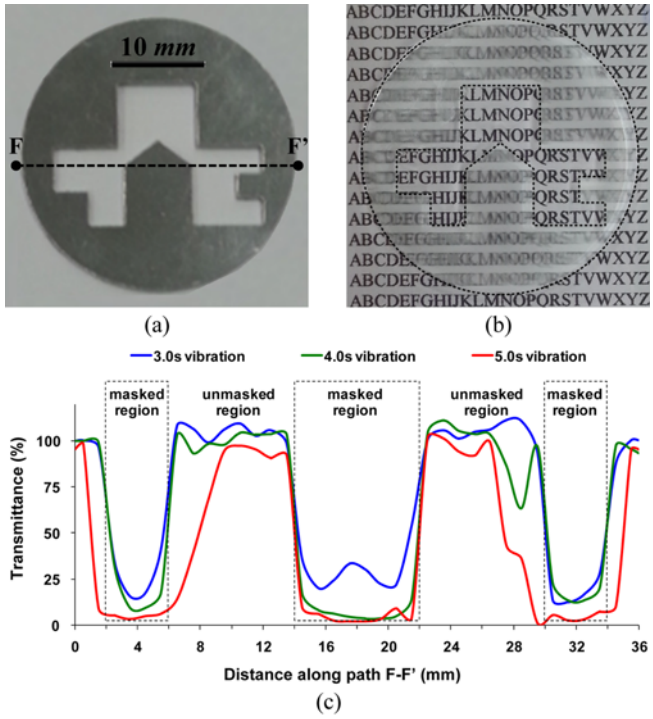

Fig. 10 Selective imprinting using an arbitrarily-shaped mask: (a) mask film with a negative logo profile, (b) replicated polymer film, and (c) transmittance comparison of the replicated films for various vibration time (F-F' section)

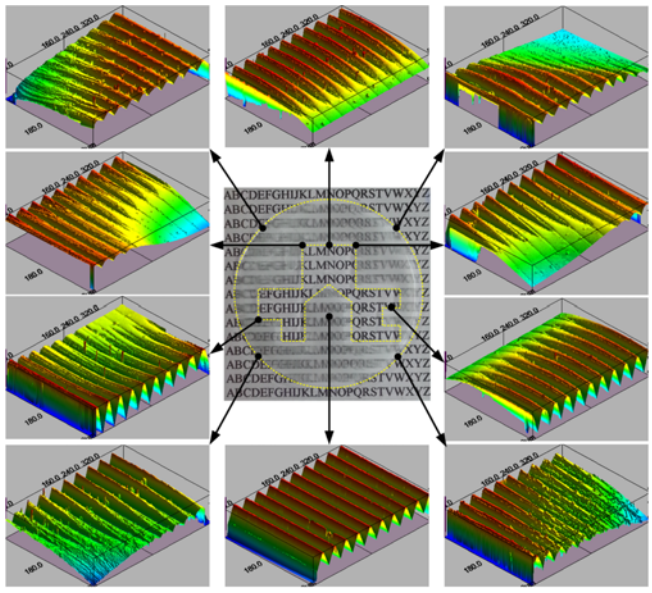

Fig. 11 Surface profiles of the replicated micropatterns at various locations on the logo (vibration time: 4.0 s)

were applied.

To investigate the change in chemical composition of the imprinted film, the surface composition of the imprinted films were analyzed using Fourier transform infrared (FT-IR) spectroscopy. FT-IR analyses were performed using a VERTEX 70v (BRUKER, Germany). The resulting

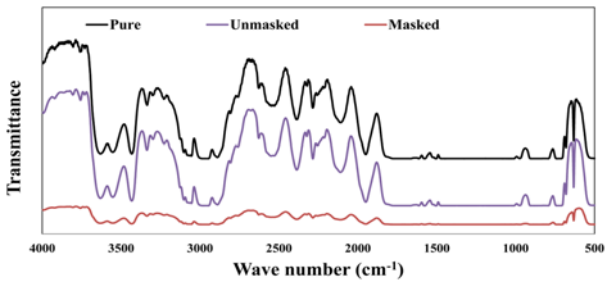

Fig. 12 Comparison of FT-IR spectra of masked and unmasked regions of imprinted PET film (vibration time: 4.0 s)

spectra for the masked and unmasked regions of the imprinted film were analyzed and compared with that of pure PET film. Fig. 12 shows the FT-IR spectra for the three types of samples. While the imprinted sample from the unmasked region shows almost the same trend as the pure PET sample, the sample from the masked region shows much lower peaks than the other two samples. This can be explained by light scattering from the replicated micropatterns. However, it can be concluded that a change in composition did not occur even in the masked region because the peak locations remained the same as those from the other two cases.

5. Conclusions

In the present study, the selective ultrasonic imprinting process was analyzed by investigating its heating mechanism in selective micropattern replication. To investigate the heating mechanism of the selective imprinting process, a coupled numerical analysis was conducted by connecting structural wave-propagation analysis and transient heat-transfer analysis. The simulation results showed that repetitive deformation and the related heat generation occurred locally in the masked regions. This localized heating enabled to raise the polymer temperature to higher than T_g within a short period (just 1.0 second in the case of the E-shaped mask). The validity of the proposed simulation was verified by experimental comparison, which showed a small amount of deviation in their maximum temperature predictions (around 7°C).

Micropatterns were then selectively replicated using an E-shaped negative mask. Ultrasonic imprinting was performed with a range of increasing vibration times, from which a moderate imprinting condition was determined not only to improve the replication characteristics in the masked region, but also to prevent excessive replication in the unmasked region. The selective imprinting process was then applied to micropattern replication of an arbitrarily shaped logo, from which optical characteristics of the replica could be differentiated in a single film. Based on these results, the proposed selective imprinting process has the versatility to allow fabrication of a variety of functional surfaces containing micropatterns, in regions with arbitrary shapes.

ACKNOWLEDGEMENT

This research was financially supported by National Research Foundation of Korea (NRF) grants funded by the Ministry of Education, Republic of Korea (Grant number: NRF-2013 R1A1A2A10004709).

REFERENCES

1. Sackmann, J., Burlage, K., Gerhardy, C., Memering, B., Liao, S., and Schomburg, W., "Review on Ultrasonic Fabrication of Polymer Micro Devices," Ultrasonics, Vol. 56, pp. 189-200, 2015.
2. Mekaru, H., Goto, H., and Takahashi, M., "Development of Ultrasonic Micro Hot Embossing Technology," Microelectronic Engineering, Vol. 84, No. 5, pp. 1282-1287, 2007.
3. Chu, W.-S., Kim, C.-S., Lee, H.-T., Choi, J.-O., Park, J.-I., et al., "Hybrid Manufacturing in Micro/Nano Scale: A Review," Int. J. Precis. Eng. Manuf.-Green Tech., Vol. 1, No. 1, pp. 75-92, 2014.
4. Chang, C.-Y. and Yu, C.-H., "A Basic Experimental Study of Ultrasonic Assisted Hot Embossing Process for Rapid Fabrication of Microlens Arrays," Journal of Micromechanics and Microengineering, Vol. 25, No. 2, Paper No. 025010, 2015.
5. Michaeli, W., Kamps, T., and Hopmann, C., "Manufacturing of Polymer Micro Parts by Ultrasonic Plasticization and Direct Injection," Microsystem Technologies, Vol. 17, No. 2, pp. 243-249, 2011.
6. Sacristan, M., Planta, X., Morell, M., and Puiggali, J., "Effects of Ultrasonic Vibration on the Micro-Molding Processing of Polylactide," Ultrasonics Sonochemistry, Vol. 21, No. 1, pp. 376-386, 2014.
7. Mekaru, H. and Takahashi, M., "Ultrasonic Nanoimprint on Poly (Ethylene Terephthalate) at Room Temperature," Japanese Journal of Applied Physics, Vol. 47, No. 6S, pp. 5178-5184, 2008.
8. Seo, Y.-S. and Park, K., "Direct Patterning of Micro-Features on a Polymer Substrate using Ultrasonic Vibration," Microsystem Technologies, Vol. 18, No. 12, pp. 2053-2061, 2012.
9. Jung, W. and Park, K., "Selective Ultrasonic Imprinting for Micropattern Replication on Predefined Area," Ultrasonics, Vol. 54, No. 6, pp. 1495-1503, 2014.
10. Lee, H.-J. and Park, K., "Development of Composite Micro-Patterns on Polymer Film using Repetitive Ultrasonic Imprinting," Int. J. Precis. Eng. Manuf.-Green Tech., Vol. 1, No. 4, pp. 341-345, 2014.
11. Park, J. H., Lee, K. Y., and Park, K., "Coupled Numerical Analysis to Investigate the Heating Mechanism of Ultrasonic Imprint Lithography," Ultrasonics, Vol. 60, pp. 96-102, 2015.
12. Nonhof, C. J. and Luiten, G. A., "Estimates for Process Conditions during the Ultrasonic Welding of Thermoplastics," Polymer Engineering & Science, Vol. 36, No. 9, pp. 1177-1183, 1996.
13. Acquasanta, F., Berti, C., Colonna, M., Fiorini, M., and Karanam, S., "Study of Glow Wire Ignition Temperature (GWIT) and Comparative Tracking Index (CTI) Performances of Engineering Thermoplastics and Correlation with Material Properties," Polymer Degradation and Stability, Vol. 96, No. 4, pp. 566-573, 2011.